

Spontaneous Formation of 2D/3D Heterostructures on the Edges of 2D Ruddlesden–Popper Hybrid Perovskite Crystals

Zhaojun Qin, Shenyu Dai, Chalapathi Charan Gajjela, Chong Wang, Viktor G. Hadjiev, Guang Yang, Jiabing Li, Xin Zhong, Zhongjia Tang, Yan Yao, Arnold M. Guloy, Rohith Reddy, David Mayerich, Liangzi Deng, Qingkai Yu, Guoying Feng, Hector A. Calderon, Francisco C. Robles Hernandez, Zhiming M. Wang,* and Jiming Bao*



Cite This: *Chem. Mater.* 2020, 32, 5009–5015



Read Online

ACCESS |



Metrics & More

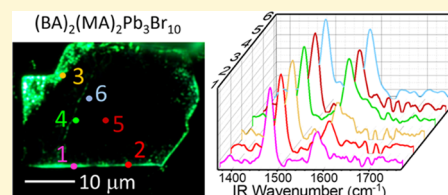


Article Recommendations



Supporting Information

ABSTRACT: The observation of low-energy edge photoluminescence and its beneficial effect on the solar cell efficiency of Ruddlesden–Popper perovskites has unleashed an intensive research effort to reveal its origin. This effort, however, has been met with more challenges as the underlying material structure has still not been identified; new modelings and observations also do not seem to converge. Using two-dimensional (2D) $(\text{BA})_2(\text{MA})_2\text{Pb}_3\text{Br}_{10}$ as an example, we show that three-dimensional (3D) MAPbBr_3 is formed due to the loss of BA on the edge. This self-formed MAPbBr_3 can explain the reported edge emission under various conditions, while the reported intriguing optoelectronic properties such as fast exciton trapping from the interior 2D perovskite, rapid exciton dissociation, and long carrier lifetime can be understood via the self-formed 2D/3D lateral perovskite heterostructure. The 3D perovskite is identified by submicron infrared spectroscopy, the emergence of X-ray diffraction (XRD) signature from freezer-milled nanometer-sized 2D perovskite, and its photoluminescence response to external hydrostatic pressure. The revelation of this edge emission mystery and the identification of a self-formed 2D/3D heterostructure provide a new approach to engineering 2D perovskites for high-performance optoelectronic devices.



INTRODUCTION

Two-dimensional (2D) Ruddlesden–Popper (RP) hybrid perovskites are stacks of atomically thin layers of three-dimensional (3D) perovskites separated by organic long-chain cations. Because of their organic spacers leading to higher material stability than that of their 3D counterparts,^{1,2} RP perovskites have attracted a lot of attention and have been used to fabricate high-performance solar cells, light-emitting diodes (LED), and photodetectors.^{1–15} RP perovskites are also an ideal platform for people to explore fundamental physics and do band-gap engineering: by tuning the thickness of layers, the band-gap and exciton binding energies can be tuned as in semiconductor quantum wells and superlattices.^{2–4,13,16} Recent surprising observations of intriguing edge photoluminescence (PL) and its benefits to solar cells have attracted more attention over the past several years.¹⁷ However, the microscopic structure of the potential edge state has not been identified and the origin of the edge emission remains controversial despite many efforts from both theoretical and experimental groups.^{18–23}

The mystery began in 2017 when Blancon et al. reported a potential edge state, which exhibited a lower-energy photoluminescence (PL) than that of exfoliated RP perovskites $(\text{BA})_2(\text{MA})_{n-1}\text{Pb}_n\text{I}_{3n+1}$ on its edge when $n \geq 3$.¹⁷ This edge state is further shown to trap photoexcited excitons from the interior of the perovskite and dissociate them into long-lived

free carriers. By orienting edges of RP perovskites along the direction of the photocurrent, a higher solar cell efficiency was achieved.¹⁷ This finding was very surprising, because edges, like grain boundaries, break crystal symmetry, and they are typically the sources of defect states and are detrimental to the device performances. However, the origin of the edge photoluminescence and its underlying microstructure were not understood and identified.¹⁷ After that, five related papers have been published to try to either solve this mystery or report new interesting physics,^{18–22} but their results do not converge, making the puzzle more difficult to solve. Two of them are theoretical papers, and they proposed very different models. Blancon and his collaborators first proposed that the edge emission and edge state are induced by strain relaxation only when $n \geq 3$.¹⁸ Later, Zhang et al., however, proposed that it is the difference in chemistry between Pb and iodine on the edge that leads to exciton dissociation and localization.²¹ In both cases, the edge states are an intrinsic property of 2D

Received: February 2, 2020

Revised: May 20, 2020

Published: May 21, 2020



perovskites. Experiments, however, point to the opposite direction and suggest that the edge emissions are extrinsic and can be controlled by external environments or chemistry. In 2019, Shi et al. reported that the edge emission was induced by moisture; they further observed the edge emission when $n = 2$ in different perovskites such as $\text{BA}_2\text{FAPb}_2\text{Br}_7$ and $\text{BA}_2\text{FAPb}_2\text{I}_7$, in conflict with the earlier observation and theory.¹⁹ Later in the same year, Zhao et al. reported the control of the edge emission by BAI and MAI.²⁰ Very recently, Wang et al. discovered that the edge has a much higher electrical conductivity than the center region.²²

It is not surprising that the origin of the edge emission remains mysterious despite these intensive efforts. The main reason is the lack of identification of the underlying structure.²³ Although transmission electron microscopy (TEM) was employed and found some differences between the edge and the center, no definite structure was identified.¹⁹ Certainly, the large discrepancies among different theories and observations described above have made it more difficult to resolve this mystery.^{18–22} In this work, we report the resolution of this mystery and identification of the underlying structure: it is the 3D perovskite and the 2D/3D perovskite heterostructure that are responsible for the lower-energy edge emission and many intriguing and beneficial optoelectronic properties. Three-dimensional perovskite is naturally formed after the loss or replacement of BA and subsequent connection of lead halide octahedrons in the vertical direction. Its identification is made possible by a combination of conventional techniques and novel approaches, which include the X-ray diffraction (XRD) of freezer-milled 2D perovskite, infrared spectroscopy at the sub-micrometer scale, and characteristic response of photoluminescence to hydrostatic pressure in a diamond anvil cell (DAC).^{24,25}

RESULTS AND DISCUSSION

As the first piece of evidence, we noticed that the reported edge PL peaks in the exfoliated 2D perovskites are always similar to those of the corresponding 3D perovskites and are independent of the layer thickness n . For example, the PL peak in the edge of $(\text{BA})_2(\text{MA})_{n-1}\text{Pb}_n\text{Br}_{3n+1}$ ($n = 3–5$) is centered at ~ 740 nm (1.68 eV),^{17,19,20,22} close to that of the PL in 3D MAPbI_3 (~ 770 nm).^{26–29} Exfoliated 2D $(\text{BA})_2(\text{MA})_{n-1}\text{Pb}_n\text{Br}_{3n+1}$ ($n = 2, 3$) exhibited an edge emission at ~ 520 nm,¹⁹ while the PL of the corresponding 3D MAPbBr_3 is centered at ~ 550 nm.^{30–33} The edge PLs of $(\text{BA})_2\text{FAPb}_2\text{I}_7$ and $(\text{BA})_2\text{FAPb}_2\text{Br}_7$ are centered at 750 and 525 nm, respectively,¹⁹ very close to 800 and 540 nm of their 3D counterparts.^{34–36}

To provide our own evidence, we synthesized representative RP perovskites $(\text{BA})_2(\text{MA})_{n-1}\text{Pb}_n\text{Br}_{3n+1}$ ($n = 1, 2, 3$) from a stoichiometric reaction in hydrobromic acid between PbO (will react with the HBr solution to produce PbBr_2), MABr , and BABr .^{4,19} The PL images and peak positions of $(\text{BA})_2(\text{MA})_{n-1}\text{Pb}_n\text{Br}_{3n+1}$ ($n = 1, 2, 3$) in Figure 1 confirm the edge emission for $n = 2$ and 3 only, in agreement with the previous report.¹⁹ Scanning electron microscopy (SEM) images in Figure 1j,k also confirm that emissive edges $(\text{BA})_2(\text{MA})_2\text{Pb}_3\text{Br}_{10}$ are smooth, as opposed to the rough edge in CsPb_2Br_5 platelets, suggesting that the edge emission does not come from the overgrown or contaminated nanostructures during the synthesis.²⁴ To determine whether the edge emission is an intrinsic or extrinsic property of the RP perovskites, we created fresh edges from a large piece of

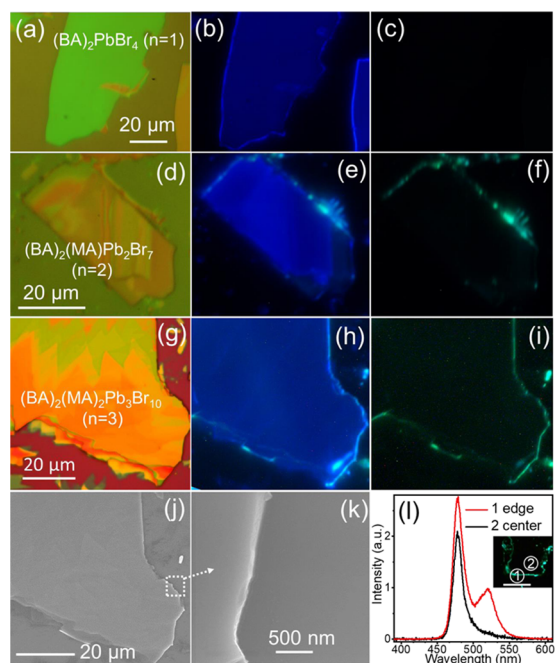


Figure 1. (a–i) Optical images (a, d, g), 365 nm UV-excited PL images with 420 nm (b, e, h), and 500 nm (c, f, i) long-pass filters of exfoliated $(\text{BA})_2(\text{MA})_{n-1}\text{Pb}_n\text{Br}_{3n+1}$ for $n = 1$ (a–c), $n = 2$ (d–f), and $n = 3$ (g–i). (j, k) Low- (j) and high- (k)-magnification SEM images of the $n = 3$ perovskite in (g)–(i). (l) Representative PL spectra of $n = 3$ perovskite from the edge and center regions, as indicated in the PL image in the inset.

$(\text{BA})_2(\text{MA})_2\text{Pb}_3\text{Br}_{10}$ using the tip of a probe and monitored its edge emission. Figure S1 and the attached video show that the PL emission from the fresh edges became stronger over time in air, indicating that the edge emission is not an intrinsic property, as proposed by two theory papers.^{18,21} In the following experiments, we will use $(\text{BA})_2(\text{MA})_2\text{Pb}_3\text{Br}_{10}$ to prove the existence of 3D MAPbBr_3 on the edge.

X-ray diffraction (XRD) is the most reliable technique to confirm and identify a material or structure; however, a direct X-ray survey in Figure S3 shows no sign of 3D MAPbBr_3 in the as-grown $(\text{BA})_2(\text{MA})_2\text{Pb}_3\text{Br}_{10}$. This is because the sensitivity of XRD is too low to detect a trace amount of the 3D structure on the edge.²³ This problem can be overcome by making smaller-sized 2D perovskites so that the surface (edge)-to-volume ratio can be significantly increased. Here, we chose a freezer mill at a liquid nitrogen temperature to physically break large bulk crystals to smaller disks without causing any chemical or compositional changes. Note that samples were loaded in and unloaded out from the milling vial in ambient air; PL and XRD measurements of the milled samples were also performed in air, so the freezer mill just acts like the probe used above to create more fresh edges.

PL images in Figure 2a,b,d reveal that these physically size-reduced RP perovskites still show a green edge emission as initial large-sized crystals. As the milling time increases from 5 to 30 min, the average size of the perovskite is further reduced to the optical diffraction limit, edge emission becomes difficult to resolve, and PL is dominated by a stronger green emission. SEM images in Figure 2c,e,f show that the surfaces and edges of these size-reduced perovskites are still exceedingly smooth as before. XRD in Figure 2g confirms that this relative increase in the green edge emission is accompanied by the emergence

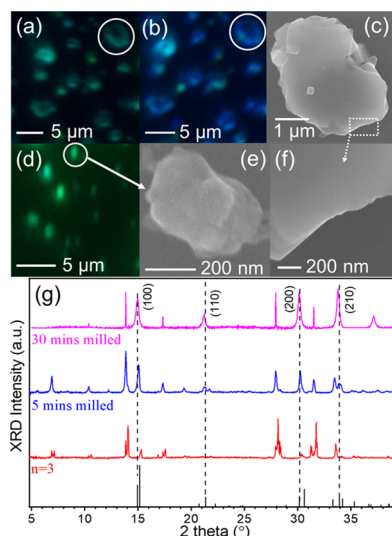


Figure 2. PL images, SEM, and XRD of freezer-milled $(\text{BA})_2(\text{MA})_2\text{Pb}_3\text{Br}_{10}$. (a, b) PL images of a 5 min milled $(\text{BA})_2(\text{MA})_2\text{Pb}_3\text{Br}_{10}$ with a 500 nm (a) and 420 nm (b) long-pass filter. (c, f) SEM of a $(\text{BA})_2(\text{MA})_2\text{Pb}_3\text{Br}_{10}$ platelet marked in (a) and (b). (d, e) PL and SEM images of a 30 min milled $(\text{BA})_2(\text{MA})_2\text{Pb}_3\text{Br}_{10}$. (g) Evolution of XRD of $(\text{BA})_2(\text{MA})_2\text{Pb}_3\text{Br}_{10}$ before and after milling for 5 and 30 min.

of the XRD pattern of 3D MAPbBr_3 . After milling for 30 min, the XRD is dominated by 3D MAPbBr_3 . Based on the XRD line width, the size of the 3D MAPbBr_3 is estimated to be ~ 28 nm. From the strong correlation between the green edge emission and XRD of MAPbBr_3 , we can conclude that the green edge emission in $(\text{BA})_2(\text{MA})_2\text{Pb}_3\text{Br}_{10}$ is due to MAPbBr_3 on the edges. We have also excluded the other two models, i.e., the strain relaxation¹⁸ and chemical difference between Pb and halide,²¹ because according to these models, MAPbBr_3 should not appear in size-reduced RP crystals.³⁷

To directly confirm the edge location of MAPbBr_3 in the 2D $(\text{BA})_2(\text{MA})_2\text{Pb}_3\text{Br}_{10}$ platelets and to correlate the property (PL) with structure (MAPbBr_3) from the same spot, we turned to optical photothermal infrared spectroscopy (O-PTIR): a noninvasive submicron spatial resolution infrared spectroscopy that utilizes a tunable quantum cascade IR laser to excite a sample photothermally through infrared absorption, a visible laser (532 nm) to probe its subsequent photothermal expansion.³⁸ This is because the large difference between the 2D $(\text{BA})_2(\text{MA})_2\text{Pb}_3\text{Br}_{10}$ and 3D MAPbBr_3 is the lack of BA in MAPbBr_3 , while IR spectroscopy is very sensitive to the organic molecules. In fact, the absence of BA and even the change in the ratio of BA to MA have been already detected by Fourier transform infrared (FTIR);^{4,29,39} Figure 3a shows the FTIR of our own samples: $(\text{BA})_2(\text{MA})_{n-1}\text{Pb}_n\text{I}_{3n+1}$ for $n = 1, 2, 3$ and MAPbBr_3 for $n = \infty$. It can be seen that with increasing n , the relative intensity of the peak located at ~ 1580 cm^{-1} decreases, and the relative intensity ratio of ~ 1480 to 1580 cm^{-1} increases.^{4,39} Figure 3b,c further shows that the intensity changes of the ~ 1580 cm^{-1} peak are accompanied by the peak shifting toward 1585 cm^{-1} . These changes can be explained by our first-principles calculations (details are given in the Supporting Information). The vibration that corresponds to 1478 cm^{-1} (CH_3 vibration) is strong only in MA^+ , so the intensity of ~ 1480 cm^{-1} has no change. $(\text{BA})_2(\text{MA})_2\text{Pb}_3\text{Br}_{10}$ has two IR absorption bands at around 1580 cm^{-1} involving

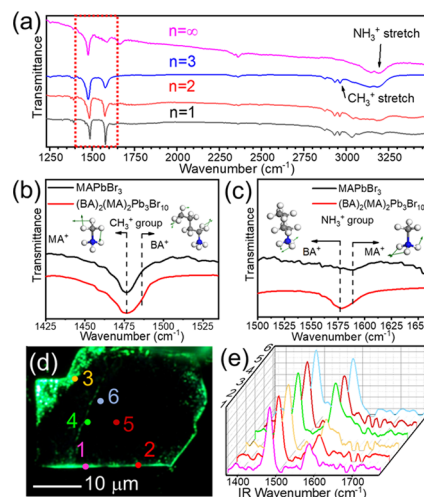


Figure 3. Identification of MAPbBr_3 on the edge by IR spectroscopy. (a) FTIR of $(\text{BA})_2(\text{MA})_{n-1}\text{Pb}_n\text{Br}_{3n+1}$ ($n = 1, 2, 3, \infty$) perovskites. (b, c) FTIR spectra of $(\text{BA})_2(\text{MA})_2\text{Pb}_3\text{Br}_{10}$ and MAPbBr_3 along with the assignment of the bands from vibration calculations of MA^+ and BA^+ molecules around 1480 cm^{-1} (b) and 1580 cm^{-1} (c). (d) PL images of $(\text{BA})_2(\text{MA})_2\text{Pb}_3\text{Br}_{10}$. (e) O-PTIR of the center regions and edges indicated in (d).

NH_3 vibrations: one band is at 1575 cm^{-1} (BA^+) and the other band at 1585 cm^{-1} (MA^+). Upon depletion of BA^+ , the band intensity at 1575 cm^{-1} decreases, leading to the reduction of the peak intensity at ~ 1580 cm^{-1} .

With the knowledge of the spectral difference between MAPbBr_3 and $(\text{BA})_2(\text{MA})_2\text{Pb}_3\text{Br}_{10}$, we used O-PTIR to compare the IR spectra between the edge and the center regions. Figure 3d,e shows three representative spots on the edge and three spots in the center. The peak intensity ratio of ~ 1480 to 1580 cm^{-1} at the edges is larger than that in the central regions. Based on O-PTIR spectra and the reported dependence of these two peak ratios on n , we obtain an $n = 5.5$ (Figure S4). This n is smaller than expected for 3D perovskite, but considering the large laser spot size of 0.5 μm and a narrow edge region,¹⁹ this number is reasonable and confirms that the edge is made of 3D perovskite.

The assignment of edge PL to MAPbBr_3 can be further confirmed by its spectral response to the external hydrostatic pressure.^{24,25} Figure 4 shows the evolution of two PL peaks under increasing pressure. It can be seen that their responses are different, and the response of the edge PL agrees well with that of the reported MAPbBr_3 : its intensity quickly decreases above 1 GPa and diminishes after 2.1 GPa. As a contrast, the

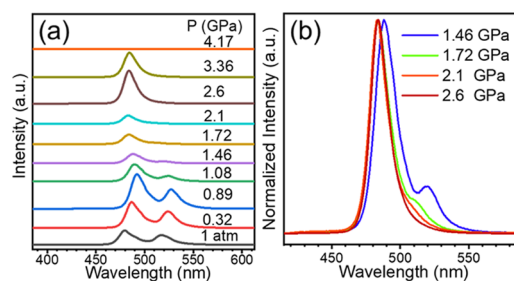


Figure 4. (a) Evolution of PL spectra and the peak position of exfoliated $(\text{BA})_2(\text{MA})_2\text{Pb}_3\text{Br}_{10}$ under hydrostatic pressure. (b) Normalized PL spectra from 1.46 to 2.6 GPa.

PL of the center region remains very strong even under 3 GPa and only disappears above 4 GPa.^{40,41}

We also measured the XRD of $(\text{BA})_2(\text{MA})_2\text{Pb}_3\text{I}_{10}$ before and after freezer-milling for 5 and 30 min. The XRD signature of 3D MAPbI_3 can be clearly seen after milling from Figure S5. Thus, the identification of 3D perovskite as a photoluminescence center for edge emission in 2D RP perovskite can explain nearly all of the reported observations. The explanation of the on/off switch of edge PL by BAI and MAI is the most straightforward as MAI can help induce MAPbI_3 on the edge and turn the edge emission on.²⁰ When exposed to humid air, both BA and MA can interact with H_2O through the H bond, but as a larger-sized spacer molecule, BA has a much weaker interaction with the lead halide octahedron frame, so BA can be lost more easily. However, a detailed microscopic picture of the degradation of RP perovskites and the associated loss of BA molecules is still missing, so further research is needed. The availability of MA and the loss of BA are necessary for the formation of MAPbX_3 , where X is a halide. That is why the edge emission can be observed when $n = 2$ but not with $n = 1$ unless MA is supplied through MAI. The blue shift of the edge emission compared to that of the PL peak of bulk 3D perovskites is due to the nanometer size of the self-formed 3D perovskite nanostructures.^{24,25,32,42} It is important to point out that a complete loss of BA and a complete conversion from 2D RP to 3D perovskites are not necessary and not possible. For large n , the distinctions between the few-layer 2D RP perovskites and 3D perovskite quantum dots are small, so the self-formed 3D perovskite nanostructures could contain a trace amount of 3D perovskite-like phases.

The formation of 3D perovskite on the edge of 2D RP perovskite leads to the creation of a lateral 2D/3D perovskite heterostructure. Many other favorable and intriguing properties can be understood from this heterostructure. Because of the lower band gap of 3D compared to that of 2D RP perovskite and their possible type-II band alignment,⁴³ photoexcited charge carriers can either be easily trapped to the 3D edge or get separated across the 2D/3D heterostructure. The dissociation of the trapped excitons and long carrier lifetime are just unique properties of the corresponding 3D perovskite.^{30,40,44,45} These interconnected 3D perovskite edges without insulating BA layers are certainly more conductive than the center regions.²² Note that the low-energy edge emissions can also be found on an imperfectly flat 2D RP surface where there are steps or terraces, as can be seen from Figures 1 and 3 of this work, as well as figures in refs 20 and 22.

CONCLUSIONS

In summary, we employed a series of well-designed experiments and proved that the self-formed 3D perovskite on the edges of 2D RP perovskites is the source of the low-energy photoluminescence. This 3D perovskite and the associated 2D/3D perovskite heterostructure are responsible for many beneficial properties that can significantly improve the efficiency of 2D perovskite solar cells. The 3D perovskite is formed after the natural loss or controlled replacement of spacer organic cations with MA. Although lead bromide perovskite is used as an example, this mechanism is applicable to other RP perovskites. 2D/3D vertical^{46–49} and lateral⁵⁰ perovskite heterostructures have been used to fabricate high-performance and stable solar cells. The identification of edge emission microstructure and understanding of its intriguing

properties of 2D/3D heterostructures will be of technological importance for the development of new optoelectronic devices based on the 2D RP hybrid perovskites.

EXPERIMENTAL DETAILS

Optical Photothermal Infrared Spectroscopy (O-PTIR). O-PTIR utilizes a tunable quantum cascade IR laser to excite a sample photothermally through infrared absorption and a 532 nm laser to probe its subsequent photothermal expansion. O-PTIR spectra of the exfoliated sample on the edge and in the center in Figure 3e were measured with a mIRage IR microscope system (Photothermal Spectroscopy Corp). The resolution of the system is 0.5 μm .

Photoluminescence (PL) Spectroscopy. PL spectra in Figure 1l were excited with a 351 nm continuous wave ion laser (Innova 300C, Coherent) and detected with a Horiba iHR320 spectrometer equipped with a Synapse CCD. A 365 nm UV LED (Thorlabs, CS2010) was used to excite samples in Figure 1b,c,e,f,h,i and the inset of Figures 1l, 2a,b,d, 3d, S1b,d–f, and S2b,d–f.

High-Pressure Diamond Anvil Cell and High-Pressure PL Spectroscopy. High-pressure PL spectra in Figure 4a were carried out with a CuBe diamond anvil cell (Diacell OmniDAC-LT model, Almax Easylabs) at room temperature. The culet of type-Ia ultralow fluorescence diamonds is 600 μm . Samples were loaded into a 250 μm hole in a BeCu gasket preindented to 70 μm , together with a ruby microsphere for pressure calibration. Silicone oil was used as a pressure-transmitting medium. The sample was excited by the 351 nm laser, and a 10 \times Mitutoyo Plan Apo objective was used to excite and collect PL.

ASSOCIATED CONTENT

Supporting Information

The Supporting Information is available free of charge at <https://pubs.acs.org/doi/10.1021/acs.chemmater.0c00419>.

Creation of fresh edges and subsequent evolution of edge photoluminescence in a $(\text{BA})_2(\text{MA})_2\text{Pb}_3\text{I}_{10}$ crystal in air (MP4)

Synthesis of bulk $(\text{BA})_2(\text{MA})_{n-1}\text{Pb}_n\text{Br}_{3n+1}$ ($n = 1, 2, 3, \infty$), scanning electron microscopy, X-ray diffraction measurements, freezer mill, Fourier transform infrared (FTIR) spectroscopy, transmission electron microscopy, molecular vibration calculations, quantification of n from the edge region, evolution of photoluminescence images of the exfoliated $(\text{BA})_2(\text{MA})_{n-1}\text{Pb}_n\text{Br}_{3n+1}$ ($n = 3$) $(\text{BA})_2(\text{MA})_{n-1}\text{Pb}_n\text{I}_{3n+1}$ ($n = 3$) crystal under UV light with a 500 nm long-pass filter, powder X-ray diffraction (XRD) of bulk $(\text{BA})_2(\text{MA})_{n-1}\text{Pb}_n\text{Br}_{3n+1}$ ($n = 1, 2, 3$) and MAPbBr_3 ($n = \infty$) perovskites, evolution of XRD of $(\text{BA})_2(\text{MA})_2\text{Pb}_3\text{I}_{10}$ before and after milling for 5 and 30 min, quantification of n from the edge region based on the ratio between 1480 and 1580 cm^{-1} peaks, and TEM of the exfoliated $(\text{BA})_2(\text{MA})_2\text{Pb}_3\text{Br}_{10}$ along the edge and in the center (PDF)

AUTHOR INFORMATION

Corresponding Authors

Jiming Bao – Department of Electrical and Computer Engineering and Materials Science & Engineering, University of Houston, Houston, Texas 77204, United States; orcid.org/0000-0002-6819-0117; Email: jbao@uh.edu

Zhiming M. Wang – Institute of Fundamental and Frontier Sciences, University of Electronic Science and Technology of China, Chengdu, Sichuan 610054, China; Email: zhmwang@uestc.edu.cn

Authors

Zhaojun Qin – Institute of Fundamental and Frontier Sciences, University of Electronic Science and Technology of China, Chengdu, Sichuan 610054, China; Department of Electrical and Computer Engineering, University of Houston, Houston, Texas 77204, United States

Shenyu Dai – Department of Electrical and Computer Engineering, University of Houston, Houston, Texas 77204, United States; College of Electronics & Information Engineering, Sichuan University, Chengdu, Sichuan 610064, China

Chalapathi Charan Gajjela – Department of Electrical and Computer Engineering, University of Houston, Houston, Texas 77204, United States

Chong Wang – Department of Electrical and Computer Engineering, University of Houston, Houston, Texas 77204, United States; School of Materials and Energy, Yunnan University, Kunming, Yunnan 650091, China

Viktor G. Hadjiev – Texas Center for Superconductivity, University of Houston, Houston, Texas 77204, United States; Department of Mechanical Engineering Technology, University of Houston, Houston, Texas 77204, United States

Guang Yang – Materials Science & Engineering, University of Houston, Houston, TX 77204, United States

Jiabin Li – Department of Electrical and Computer Engineering, University of Houston, Houston, Texas 77204, United States

Xin Zhong – Texas Center for Superconductivity, University of Houston, Houston, Texas 77204, United States; Department of Chemistry, University of Houston, Houston, Texas 77204, United States

Zhongjia Tang – Texas Center for Superconductivity, University of Houston, Houston, Texas 77204, United States; Department of Chemistry, University of Houston, Houston, Texas 77204, United States

Yan Yao – Department of Electrical and Computer Engineering, University of Houston, Houston, Texas 77204, United States

Arnold M. Guloy – Texas Center for Superconductivity, University of Houston, Houston, Texas 77204, United States; Department of Chemistry, University of Houston, Houston, Texas 77204, United States; orcid.org/0000-0003-2492-4323

Rohith Reddy – Department of Electrical and Computer Engineering, University of Houston, Houston, Texas 77204, United States

David Mayerich – Department of Electrical and Computer Engineering, University of Houston, Houston, Texas 77204, United States

Liangzi Deng – Texas Center for Superconductivity, University of Houston, Houston, Texas 77204, United States; Department of Physics, University of Houston, Houston, Texas 77204, United States

Qingkai Yu – Ingram School of Engineering, Texas State University, San Marcos, Texas 78666, United States; orcid.org/0000-0002-1859-1895

Guoying Feng – College of Electronics & Information Engineering, Sichuan University, Chengdu, Sichuan 610064, China

Hector A. Calderon – Instituto Politecnico Nacional, ESFM-IPN, Departamento de Fisica, UPALM Zacatenco, CDMX 07338, Mexico

Francisco C. Robles Hernandez – Department of Mechanical Engineering Technology, University of Houston, Houston, Texas 77204, United States

Complete contact information is available at:
<https://pubs.acs.org/10.1021/acs.chemmater.0c00419>

Notes

The authors declare no competing financial interest.

ACKNOWLEDGMENTS

J.B. acknowledges support from the Robert A. Welch Foundation (E-1728). The work by Z.M.W. is supported by the National Key Research and Development Program of China (2019YFB2203400), the “111 Project” (B20030), and the UESTC Shared Research Facilities of Electromagnetic Wave and Matter Interaction (Y0301901290100201). Z.Q. acknowledges financial support from the Academic Exchange Special Fund at the University of Electronic Science and Technology of China. C.W. is supported by Joint Foundation of Provincial Science and Technology Department-Double First-class Construction of Yunnan University [No. 2019FY003016]. R.R. Acknowledges support from CPRIT (RR170075). Work at the Molecular Foundry was supported by the Office of Science, Office of Basic Energy Sciences, of the U.S. Department of Energy under Contract No. DE-AC02-05CH11231.

REFERENCES

- (1) Dong, R.; Lan, C.; Xu, X.; Liang, X.; Hu, X.; Li, D.; Zhou, Z.; Shu, L.; Yip, S.; Li, C.; Tsang, S. W.; Ho, J. C. Novel Series of Quasi-2D Ruddlesden-Popper Perovskites Based on Short-Chained Spacer Cation for Enhanced Photodetection. *ACS Appl. Mater. Interfaces* **2018**, *10*, 19019–19026.
- (2) Stoumpos, C. C.; Soe, C. M. M.; Tsai, H.; Nie, W. Y.; Blancon, J. C.; Cao, D. Y. H.; Liu, F. Z.; Traore, B.; Katan, C.; Even, J.; Mohite, A. D.; Kanatzidis, M. G. High Members of the 2D Ruddlesden-Popper Halide Perovskites: Synthesis, Optical Properties, and Solar Cells of $(\text{CH}_3(\text{CH}_2)_3\text{NH}_3)_2(\text{CH}_3\text{NH}_3)_4\text{Pb}_5\text{I}_{16}$. *Chem* **2017**, *2*, 427–440.
- (3) Cao, D. H.; Stoumpos, C. C.; Farha, O. K.; Hupp, J. T.; Kanatzidis, M. G. 2D Homologous Perovskites as Light-Absorbing Materials for Solar Cell Applications. *J. Am. Chem. Soc.* **2015**, *137*, 7843–7850.
- (4) Stoumpos, C. C.; Cao, D. H.; Clark, D. J.; Young, J.; Rondinelli, J. M.; Jang, J. I.; Hupp, J. T.; Kanatzidis, M. G. Ruddlesden-Popper Hybrid Lead Iodide Perovskite 2D Homologous Semiconductors. *Chem. Mater.* **2016**, *28*, 2852–2867.
- (5) Li, L. N.; Sun, Z. H.; Wang, P.; Hu, W. D.; Wang, S. S.; Ji, C. M.; Hong, M. C.; Luo, J. H. Tailored Engineering of an Unusual $(\text{C}_4\text{H}_9\text{NH}_3)_2(\text{CH}_3\text{NH}_3)_2\text{Pb}_3\text{Br}_{10}$ Two-Dimensional Multilayered Perovskite Ferroelectric for a High-Performance Photodetector. *Angew. Chem., Int. Ed.* **2017**, *56*, 12150–12154.
- (6) Tsai, H.; Nie, W.; Blancon, J. C.; Stoumpos, C. C.; Soe, C. M. M.; Yoo, J.; Crochet, J.; Tretiak, S.; Even, J.; Sadhanala, A.; Azzellino, G.; Brenes, R.; Ajayan, P. M.; Bulovic, V.; Stranks, S. D.; Friend, R. H.; Kanatzidis, M. G.; Mohite, A. D. Stable Light-Emitting Diodes Using Phase-Pure Ruddlesden-Popper Layered Perovskites. *Adv. Mater.* **2018**, *30*, No. 1704217.
- (7) Cheng, P. R.; Xu, Z.; Li, J. B.; Liu, Y. C.; Fan, Y. Y.; Yu, L. Y.; Smilgies, D. M.; Muller, C.; Zhao, K.; Liu, S. F. Highly Efficient Ruddlesden-Popper Halide Perovskite $\text{PA}_2\text{MA}_4\text{Pb}_5\text{I}_{16}$ Solar Cells. *ACS Energy Lett.* **2018**, *3*, 1975–1982.
- (8) Soe, C. M. M.; Stoumpos, C. C.; Kepenekian, M.; Traore, B.; Tsai, H.; Nie, W.; Wang, B.; Katan, C.; Seshadri, R.; Mohite, A. D.; Even, J.; Marks, T. J.; Kanatzidis, M. G. New Type of 2D Perovskites with Alternating Cations in the Interlayer Space, $(\text{C}(\text{NH}_2)_3)_n(\text{CH}_3\text{NH}_3)_m\text{Pb}_{n+1}$: Structure, Properties, and Photovoltaic Performance. *J. Am. Chem. Soc.* **2017**, *139*, 16297–16309.

- (9) Tsai, H.; Nie, W.; Blancon, J. C.; Stoumpos, C. C.; Asadpour, R.; Harutyunyan, B.; Neukirch, A. J.; Verduzco, R.; Crochet, J. J.; Tretiak, S.; Pedesseau, L.; Even, J.; Alam, M. A.; Gupta, G.; Lou, J.; Ajayan, P. M.; Bedzyk, M. J.; Kanatzidis, M. G.; Mohite, A. D. High-Efficiency Two-Dimensional Ruddlesden-Popper Perovskite Solar Cells. *Nature* **2016**, *536*, 312–316.
- (10) Cohen, B.-E.; Wierzbowska, M.; Etgar, L. High Efficiency and High Open Circuit Voltage in Quasi 2D Perovskite Based Solar Cells. *Adv. Funct. Mater.* **2017**, *27*, No. 1604733.
- (11) Chen, Y. N.; Sun, Y.; Peng, J. J.; Zhang, W.; Su, X. J.; Zheng, K. B.; Pullerits, T.; Liang, Z. Q. Tailoring Organic Cation of 2D Air-Stable Organometal Halide Perovskites for Highly Efficient Planar Solar Cells. *Adv. Energy Mater.* **2017**, *7*, No. 1700162.
- (12) Byun, J.; Cho, H.; Wolf, C.; Jang, M.; Sadhanala, A.; Friend, R. H.; Yang, H.; Lee, T. W. Efficient Visible Quasi-2D Perovskite Light-Emitting Diodes. *Adv. Mater.* **2016**, *28*, 7515–7520.
- (13) Nie, L. F.; Ke, X. X.; Sui, M. L. Microstructural Study of Two-Dimensional Organic-Inorganic Hybrid Perovskite Nanosheet Degradation under Illumination. *Nanomaterials* **2019**, *9*, No. 722.
- (14) Nazarenko, O.; Kotyba, M. R.; Worle, M.; Cuervo-Reyes, E.; Yakunin, S.; Kovalenko, M. V. Luminescent and Photoconductive Layered Lead Halide Perovskite Compounds Comprising Mixtures of Cesium and Guanidinium Cations. *Inorg. Chem.* **2017**, *56*, 11552–11564.
- (15) Mao, L.; Kennard, R. M.; Traore, B.; Ke, W.; Katan, C.; Even, J.; Chabinc, M. L.; Stoumpos, C. C.; Kanatzidis, M. G. Seven-Layered 2D Hybrid Lead Iodide Perovskites. *Chem* **2019**, *5*, 2593–2604.
- (16) Dou, L. T.; Wong, A. B.; Yu, Y.; Lai, M. L.; Kornienko, N.; Eaton, S. W.; Fu, A.; Bischak, C. G.; Ma, J.; Ding, T. N.; Ginsberg, N. S.; Wang, L. W.; Alivisatos, A. P.; Yang, P. D. Atomically Thin Two-Dimensional Organic-Inorganic Hybrid Perovskites. *Science* **2015**, *349*, 1518–1521.
- (17) Blancon, J. C.; Tsai, H.; Nie, W.; Stoumpos, C. C.; Pedesseau, L.; Katan, C.; Kepenekian, M.; Soe, C. M. M.; Appavoo, K.; Sfeir, M. Y.; Tretiak, S.; Ajayan, P. M.; Kanatzidis, M. G.; Even, J.; Crochet, J. J.; Mohite, A. D. Extremely Efficient Internal Exciton Dissociation Through Edge States in Layered 2D Perovskites. *Science* **2017**, *355*, 1288–1292.
- (18) Kepenekian, M.; Traore, B.; Blancon, J. C.; Pedesseau, L.; Tsai, H.; Nie, W.; Stoumpos, C. C.; Kanatzidis, M. G.; Even, J.; Mohite, A. D.; Tretiak, S.; Katan, C. Concept of Lattice Mismatch and Emergence of Surface States in Two-dimensional Hybrid Perovskite Quantum Wells. *Nano Lett.* **2018**, *18*, 5603–5609.
- (19) Shi, E. Z.; Deng, S. B.; Yuan, B.; Gao, Y.; Akriti; Yuan, L.; Davis, C. S.; Zemlyanov, D.; Yu, Y.; Huang, L. B.; Dou, L. T. Extrinsic and Dynamic Edge States of Two-Dimensional Lead Halide Perovskites. *ACS Nano* **2019**, *13*, 1635–1644.
- (20) Zhao, C.; Tian, W.; Leng, J.; Zhao, Y.; Jin, S. Controlling the Property of Edges in Layered 2D Perovskite Single Crystals. *J. Phys. Chem. Lett.* **2019**, *10*, 3950–3954.
- (21) Zhang, Z. S.; Fang, W. H.; Long, R.; Prezhdo, O. V. Exciton Dissociation and Suppressed Charge Recombination at 2D Perovskite Edges: Key Roles of Unsaturated Halide Bonds and Thermal Disorder. *J. Am. Chem. Soc.* **2019**, *141*, 15557–15566.
- (22) Wang, K.; Wu, C. C.; Jiang, Y. Y.; Yang, D.; Wang, K.; Priya, S. Distinct Conducting Layer Edge States in Two-Dimensional (2D) Halide Perovskite. *Sci. Adv.* **2019**, *5*, No. eaau3241.
- (23) Bao, J.; Hadjiev, V. G. Origin of Luminescent Centers and Edge States in Low-Dimensional Lead Halide Perovskites: Controversies, Challenges and Instructive Approaches. *Nano-Micro Lett.* **2019**, *11*, No. 26.
- (24) Wang, C.; Wang, Y. N.; Su, X. H.; Hadjiev, V. G.; Dai, S. Y.; Qin, Z. J.; Benavides, H. A. C.; Ni, Y. Z.; Li, Q.; Jian, J.; Alam, M. K.; Wang, H. Y.; Hernandez, F. C. R.; Yao, Y.; Chen, S.; Yu, Q. K.; Feng, G. Y.; Wang, Z. M.; Bao, J. M. Extrinsic Green Photoluminescence from the Edges of 2D Cesium Lead Halides. *Adv. Mater.* **2019**, *31*, No. e1902492.
- (25) Qin, Z. J.; Dai, S. Y.; Hadjiev, V. G.; Wang, C.; Xie, L. X.; Ni, Y. Z.; Wu, C. Z.; Yang, G.; Chen, S.; Deng, L. Z.; Yu, Q. K.; Feng, G. Y.; Wang, Z. M. M.; Bao, J. M. Revealing the Origin of Luminescence Center in 0D Cs₄PbBr₆ Perovskite. *Chem. Mater.* **2019**, *31*, 9098–9104.
- (26) Park, B. W.; Jain, S. M.; Zhang, X. L.; Hagfeldt, A.; Boschloo, G.; Edvinsson, T. Resonance Raman and Excitation Energy Dependent Charge Transfer Mechanism in Halide-Substituted Hybrid Perovskite Solar Cells. *ACS Nano* **2015**, *9*, 2088–2101.
- (27) Chatterjee, S.; Pal, A. J. Introducing Cu₂O Thin Films as a Hole-Transport Layer in Efficient Planar Perovskite Solar Cell Structures. *J. Phys. Chem. C* **2016**, *120*, 1428–1437.
- (28) Wu, Y. Z.; Xie, F. X.; Chen, H.; Yang, X. D.; Su, H. M.; Cai, M. L.; Zhou, Z. M.; Noda, T.; Han, L. Y. Thermally Stable MAPbI₃ Perovskite Solar Cells with Efficiency of 19.19% and Area over 1 cm² achieved by Additive Engineering. *Adv. Mater.* **2017**, *29*, No. 1701073.
- (29) Zhu, Z.; Hadjiev, V. G.; Rong, Y. G.; Guo, R.; Cao, B.; Tang, Z. J.; Qin, F.; Li, Y.; Wang, Y. N.; Hao, F.; Venkatesan, S.; Li, W. Z.; Baldelli, S.; Guloy, A. M.; Fang, H.; Hu, Y. D.; Yao, Y.; Wang, Z. M.; Bao, J. M. Interaction of Organic Cation with Water Molecule in Perovskite MAPbI₃: From Dynamic Orientational Disorder to Hydrogen Bonding. *Chem. Mater.* **2016**, *28*, 7385–7393.
- (30) Cho, H. C.; Jeong, S. H.; Park, M. H.; Kim, Y. H.; Wolf, C.; Lee, C. L.; Heo, J. H.; Sadhanala, A.; Myoung, N.; Yoo, S.; Im, S. H.; Friend, R. H.; Lee, T. W. Overcoming the Electroluminescence Efficiency Limitations of Perovskite Light-Emitting Diodes. *Science* **2015**, *350*, 1222–1225.
- (31) Wei, H. T.; Fang, Y. J.; Mulligan, P.; Chuirazzi, W.; Fang, H. H.; Wang, C. C.; Ecker, B. R.; Gao, Y. L.; Loi, M. A.; Cao, L.; Huang, J. S. Sensitive X-ray Detectors Made of Methylammonium Lead Tribromide Perovskite Single Crystals. *Nat. Photonics* **2016**, *10*, 333–339.
- (32) Tyagi, P.; Arveson, S. M.; Tisdale, W. A. Colloidal Organohalide Perovskite Nanoplatelets Exhibiting Quantum Confinement. *J. Phys. Chem. Lett.* **2015**, *6*, 1911–1916.
- (33) Yang, Y.; Yan, Y.; Yang, M. J.; Choi, S.; Zhu, K.; Luther, J. M.; Beard, M. C. Low Surface Recombination Velocity in Solution-Grown CH₃NH₃PbBr₃ Perovskite Single Crystal. *Nat. Commun.* **2015**, *6*, No. 7961.
- (34) Fang, H. H.; Wang, F.; Adjokatsé, S.; Zhao, N.; Even, J.; Loi, M. A. Photoexcitation Dynamics in Solution-Processed Formamidinium Lead Iodide Perovskite Thin Films for Solar Cell Applications. *Light: Sci. Appl.* **2016**, *5*, No. e16056.
- (35) Tong, Y. L.; Zhang, Y. W.; Ma, K. Z.; Cheng, R.; Wang, F. X.; Chen, S. One-Step Synthesis of FA-Directing FAPbBr₃ Perovskite Nanocrystals toward High-Performance Display. *ACS Appl. Mater. Interfaces* **2018**, *10*, 31603–31609.
- (36) Hanusch, F. C.; Wiesenmayer, E.; Mankel, E.; Binek, A.; Angloher, P.; Fraunhofer, C.; Giesbrecht, N.; Feckl, J. M.; Jaegermann, W.; Johrendt, D.; Bein, T.; Docompo, P. Efficient Planar Heterojunction Perovskite Solar Cells Based on Formamidinium Lead Bromide. *J. Phys. Chem. Lett.* **2014**, *5*, 2791–2795.
- (37) Guo, X.; McCleese, C.; Kolodziej, C.; Samia, A. C. S.; Zhao, Y.; Burda, C. Identification and characterization of the intermediate phase in hybrid organic-inorganic MAPbI₃ perovskite. *Dalton Trans.* **2016**, *45*, 3806–3813.
- (38) Zhang, D. L.; Li, C.; Zhang, C.; Slipchenko, M. N.; Eakins, G.; Cheng, J. X. Depth-resolved mid-infrared photothermal imaging of living cells and organisms with submicrometer spatial resolution. *Sci. Adv.* **2016**, *2*, No. e1600521.
- (39) Soe, C. M. M.; Nagabhushana, G. P.; Shivaramaiah, R.; Tsai, H. H.; Nie, W. Y.; Blancon, J. C.; Melkonyan, F.; Cao, D. H.; Traore, B.; Pedesseau, L.; Kepenekian, M.; Katan, C.; Even, J.; Marks, T. J.; Navrotsky, A.; Mohite, A. D.; Stoumpos, C. C.; Kanatzidis, M. G. Structural and Thermodynamic Limits of Layer Thickness in 2D Halide Perovskites. *Proc. Natl. Acad. Sci. U.S.A.* **2019**, *116*, 58–66.
- (40) Yin, T. T.; Fang, Y. N.; Chong, W. K.; Ming, K. T.; Jiang, S. J.; Li, X. L.; Kuo, J. L.; Fang, J. Y.; Sum, T. C.; White, T. J.; Yan, J. X.

Shen, Z. X. High-Pressure-Induced Comminution and Recrystallization of $\text{CH}_3\text{NH}_3\text{PbBr}_3$ Nanocrystals as Large Thin Nanoplates. *Adv. Mater.* **2018**, *30*, No. 1705017.

(41) Wang, Y. H.; Lu, X. J.; Yang, W. G.; Wen, T.; Yang, L. X.; Ren, X. T.; Wang, L.; Lin, Z. S.; Zhao, Y. S. Pressure-Induced Phase Transformation, Reversible Amorphization, and Anomalous Visible Light Response in Organolead Bromide Perovskite. *J. Am. Chem. Soc.* **2015**, *137*, 11144–11149.

(42) Droseros, N.; Longo, G.; Brauer, J. C.; Sessolo, M.; Bolink, H. J.; Banerji, N. Origin of the Enhanced Photoluminescence Quantum Yield in MAPbBr_3 Perovskite with Reduced Crystal Size. *ACS Energy Lett.* **2018**, *3*, 1458–1466.

(43) Wang, J.; Leng, J.; Liu, J.; He, S.; Wang, Y.; Wu, K.; Jin, S. Engineered Directional Charge Flow in Mixed Two-Dimensional Perovskites Enabled by Facile Cation-Exchange. *J. Phys. Chem. C* **2017**, *121*, 21281–21289.

(44) Han, D. B.; Imran, M.; Zhang, M. J.; Chang, S.; Wu, X. G.; Zhang, X.; Tang, J. L.; Wang, M. S.; Ali, S.; Li, X. G.; Yu, G.; Han, J. B.; Wang, L. X.; Zou, B. S.; Zhong, H. Z. Efficient Light-Emitting Diodes Based on in Situ Fabricated FAPbBr_3 Nanocrystals: The Enhancing Role of the Ligand-Assisted Reprecipitation Process. *ACS Nano* **2018**, *12*, 8808–8816.

(45) Hsu, H. Y.; Ji, L.; Du, M. S.; Zhao, J.; Yu, E. T.; Bard, A. J. Optimization of $\text{PbI}_2/\text{MAPbI}_3$ Perovskite Composites by Scanning Electrochemical Microscopy. *J. Phys. Chem. C* **2016**, *120*, 19890–19895.

(46) Wang, Z. P.; Lin, Q. Q.; Chmiel, F. P.; Sakai, N.; Herz, L. M.; Snaith, H. J. Efficient Ambient-Air-Stable Solar Cells With 2D-3D Heterostructured Butylammonium-Caesium-Formamidinium Lead Halide Perovskites. *Nat. Energy* **2017**, *2*, No. 17135.

(47) Zhang, T.; Xie, L.; Chen, L.; Guo, N.; Li, G.; Tian, Z.; Mao, B.; Zhao, Y. In Situ Fabrication of Highly Luminescent Bifunctional Amino Acid Crosslinked 2D/3D $\text{NH}_3\text{C}_4\text{H}_9\text{COO}(\text{CH}_3\text{NH}_3\text{PbBr}_3)_n$ Perovskite Films. *Adv. Funct. Mater.* **2017**, *27*, No. 1603568.

(48) Liu, B. A.; Long, M. Q.; Cai, M. Q.; Ding, L. M.; Yang, J. L. Interfacial Charge Behavior Modulation in 2D/3D Perovskite Heterostructure for Potential High-Performance Solar Cells. *Nano Energy* **2019**, *59*, 715–720.

(49) Yang, F.; Zhang, P. T.; Kamarudin, M. A.; Kapil, G.; Ma, T. L.; Hayase, S. Addition Effect of Pyreneammonium Iodide to Methylammonium Lead Halide Perovskite-2D/3D Heterostructured Perovskite with Enhanced Stability. *Adv. Funct. Mater.* **2018**, *28*, No. 1804856.

(50) Li, P. W.; Zhang, Y. Q.; Liang, C.; Xing, G. C.; Liu, X. L.; Li, F. Y.; Liu, X. T.; Hu, X. T.; Shao, G. S.; Song, Y. L. Phase Pure 2D Perovskite for High-Performance 2D-3D Heterostructured Perovskite Solar Cells. *Adv. Mater.* **2018**, *30*, No. e1805323.